A Self-Adapting Synchronized-Switch Interface Circuit for Piezoelectric Energy Harvesters

Salar Chamanian, *Student Member, IEEE*, Ali Muhtaroğlu, *Senior Member, IEEE*, and Haluk Külah, *Member, IEEE*

***Abstract*—This paper presents a self-adapting synchronized-switch harvesting (SA-SSH) interface circuit to extract energy from vibration-based piezoelectric energy harvesters (PEHs). The implemented circuit utilizes a novel switching technique to recycle optimum amount of harvested charge on piezoelectric capacitance to strengthen the damping force, and simultaneously achieve load-independent energy extraction with a single inductor. Charge recycling is realized by adjusting extraction time, and optimized through a maximum power point tracker based on charge-flipping dissipation. The circuit has been implemented using 180 nm HV CMOS technology with 0.9 $\times$ 0.6 mm^2 active area. Self-adapting SSH circuit has been validated with both macro-scaled and MEMS PEHs with different inductor values. The interface circuit provides maximum energy extraction for the full storage voltage range of 1.8–3.7 V. The implementation harnesses have 500% more power compared to an ideal full-bridge rectifier, and output 3.4 μW for 2.24 V peak-to-peak open-circuit piezoelectric voltage from MEMS PEH excited at its resonant frequency.**

***Index Terms*—Maximum power point tracker (MPPT), piezoelectric energy harvester (PEH), self-adapting synchronized-switch harvesting (SA-SSH), self-adapting, vibration.**

I. Introduction

MINIATURIZATION in microelectronic systems, such as wireless and implantable sensors, demands increasingly stringent battery size provisions. Such systems contrarily require large energy sources for prolonged operation with low maintenance in order to achieve low cost. Microelectronics hence starts making use of energy-harvesting systems to achieve reliable operation over long periods, and reduce system costs [1], [2]. Harvesting energy from environmental vibration is of great interest in self-sustained systems due to its abundance and availability. Piezoelectric transducers are widely utilized in generating electrical energy from vibrations, due to their relatively high power density, scalability, and compatibility with integrated circuits (ICs). Several MEMS piezoelectric transducers were fabricated in the past [3], [4], which could harvest power between few micro watts to hundreds of micro watts from ambient vibrations. piezoelectric energy harvesters (PEHs) generate ac power, and have relatively high capacitive output impedance. Therefore, it is necessary to interface the PEH in a microelectronic system with a special IC that is capable of power management to attain a regulated standard dc voltage and efficient energy extraction [5], [6].

Active rectifiers were commonly employed to reduce power dissipation in the interface circuit for improved efficiency [7], [8]. However, these circuits suffer from reactive power dissipation due to capacitive impedance of the PEH. MPPT circuits were proposed in [9], [10] to improve power efficiency. Nevertheless, these circuits focused on matching real part of the source impedance, and thus could not prevent wasting significant amount of transient charge at piezoelectric capacitance. Nonlinear processing of piezoelectric voltage was employed in the past to overcome such issues and maximize energy extraction, 1) in synchronous electric charge extraction (SECE) by establishing a resonant circuit between piezoelectric capacitance and an external inductor, and 2) in synchronized switch harvesting on inductor (SSHI). Theoretical analyses conducted by [11], [12] show that SECE and SSHI can increase extracted power up to 400% and 900%, respectively, compared to a full-bridge rectifier. For low-coupled or off-resonance harvesters, SECE [13], [14] is an efficient switching approach that extracts and transfers energy to an inductor in synchrony with available charge on piezoelectric harvester. SECE technique provides load independence, and facilitates charge delivery to the storage capacitor. Fully self-powered and improved versions of the SECE were demonstrated in [13], [15]. SSHI technique was proposed in [16] to perform charge inversion on piezoelectric capacitance to transfer energy to the storage device with minimal charge dissipation at the rectifier. However, the output power of the SSHI depends strongly on output load, and high efficiency can only be attained in limited range of excitation levels. Several adaptations [17], [18] and on-chip implementations [19]–[21] were presented to enhance performance of the SSHI rectifier. Nevertheless, the adaptability of the aforementioned rectifiers to variations of the input power level or harvesters has not been reported [19], [21]. On the other hand, charge inversion method requires cumbersome adjustments [19], [21], [22]. Recent studies [23]

Manuscript received November 26, 2018; revised February 15, 2019; accepted March 29, 2019. Date of publication May 2, 2019; date of current version October 18, 2019. This work was supported by FLAMENCO project, funded by European Research Council (ERC) under the European Union's Horizon 2020 research and innovation programme under Grant 682756. Recommended for publication by Associate Editor M. Anderson. *(Corresponding author: Salar Chamanian.)*

S. Chamanian is with the Department of Electrical and Electronics Engineering, Middle East Technical University, Ankara 06800, Turkey (e-mail: salar.chamanian@metu.edu.tr).

A. Muhtaroğlu is with the Department of Electrical and Electronics Engineering and also with the Center for Sustainability, Middle East Technical University Northern Cyprus Campus, Güzelyurt, Mersin 10 Turkey (e-mail: amuhtar@metu.edu.tr).

H. Külah is with the Department of Electrical and Electronics Engineering, Middle East Technical University, Ankara 06800, Turkey, and also with the METU-MEMS Research and Application Center, Ankara 06800, Turkey (e-mail: kulah@metu.edu.tr).

Color versions of one or more of the figures in this paper are available online at http://ieeexplore.ieee.org.

Digital Object Identifier 10.1109/TPEL.2019.2910410

and [24] utilized multielectrodes PEH to facilitate start-up of the IC and voltage current ratio of the PEH, respectively, with the conventional SSHI core circuit, which include the same concerns. Although Wu [25] proposed a method using active diodes to secure optimal timing of charge inversion, the improvement of extraction power was not considerable compared to the ideal upper limit. Inductorless designs presented in [26] and [27] utilize charge-flipping capacitors instead of inductors to flip voltages, which can lead to shrinking the system volume. Flipping capacitor size depends on the piezoelectric capacitor value and several numbers of the capacitor are required to achieve high flipping efficiency. Hence, numerous switches required by such approaches curtail power conversion efficiency and extracted output power severely due to high switching losses. Moreover, interface circuits in [26] and [27] need external calibration of charge-flipping time to obtain maximum output power for each PEH type and environmental conditions, and output power strongly depends on the output load.

The aim of this paper is to integrate a self-adapting interface circuit to boost extracted power from small-to-medium size electromechanically coupled PEHs. The implementation of an improved switching technique based on synchronized switching provides high power extraction gain and load independence simultaneously with a single inductor. The low power design enables efficient operation with a wider range of excitation frequency and output storage voltage. Furthermore, for the first time in literature a novel MPP sensing approach is proposed, and implemented to achieve optimal point of operation for the proposed circuit regardless of input excitation level. SA-SSH fundamentals are introduced in the next section. Section III provides circuit implementation details. Design validation results follow in Section IV from a fabricated test chip. Finally, conclusions from this paper are summarized.

II. SA-SSH Interface Circuit

A. Concept and Operation Principle

Recycling or investing charge on piezoelectric material to increase damping force is essential to increase extracted power. Energy recycling can be realized through flipping charge on piezoelectric capacitance, C_P, as a result of establishing a resonant circuit between C_P and an external inductor, *L*. The energy stored in C_P is transferred to the inductor, and back to the capacitor to flip the capacitor voltage to $-\lambda V_P$. The efficiency of charge flipping is mainly constrained by the quality factor (*Q*) of the *RLC*, and the topology of the harvesting circuit. Fig. 1 shows an *RLC* resonant circuit, where *r* stands for the parasitic resistance along the loop comprising the parasitic resistance of the inductor (*L*), and the switch. The *Q* factor and damped resonant frequency of the path are given as

$$Q = \frac{1}{r}\sqrt{\frac{L}{C_p}} \tag{1}$$

$$\omega_d = \sqrt{\frac{1}{LC_p} - \frac{r^2}{4L^2}}. \tag{2}$$

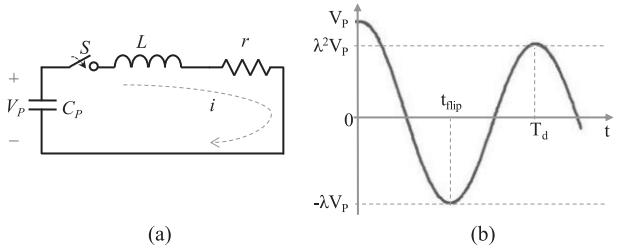

Fig. 1. (a) *RLC* resonant circuit established in charge filliping. (b) Capacitor voltage.

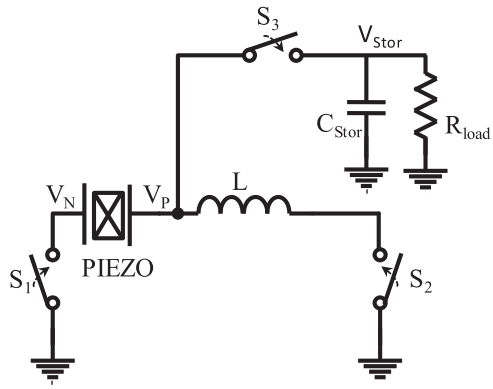

Fig. 2. Schematic of proposed circuit.

Let us consider that the initial value of the capacitor is V_P and the switch S is closed at $t = 0$. The fraction of voltage conserved on the capacitor of an *RLC* oscillator with quality factor *Q* is $\lambda = e^{-\frac{\pi}{2Q}}$ after half cycle of damped resonance period. Indeed, the capacitor voltage flips with λ factor within time $t_{\text{flip}} = \frac{\pi}{\omega_d}$. As *Q* rises, λ gets closer to one; and so does the efficiency of the SSHI circuits. The proposed circuit uses charge-flipping technique to recycle optimum charge into the piezoelectric capacitance, which enables significant improvement in energy extraction from the harvester.

Fig. 2 shows a model for the proposed interface circuit. The nonlinear processing circuit is only composed of an inductor *L* in series with electronic switches S_1, S_2, and in parallel with an energy transfer switch S_3. The piezoelectric harvester is simply modeled by an alternating current source in parallel with a capacitance of the piezoelectric material (C_P) to illustrate piezoelectric behavior and circuit operation as shown in Fig. 3. Fig. 3(a) depicts the waveforms for mechanical displacement, piezoelectric voltage, V_{PZT}, and inductor current, I_{IND}. Fig. 3 (b) presents the operation phases of the switching circuit for an excitation cycle.

1) Initially, positive charge is generated on piezoelectric capacitance, as harvester current is positive, which represents upward strain on piezoelectric material. In this case, S_1 is ON to connect V_N node to ground, while S_2 is OFF to block current flow into the inductor.
2) S_2 switch turns ON when the mechanical displacement reaches its peak value. At this time, an oscillating electrical circuit L–C_P is established and S_1 switch is turned OFF

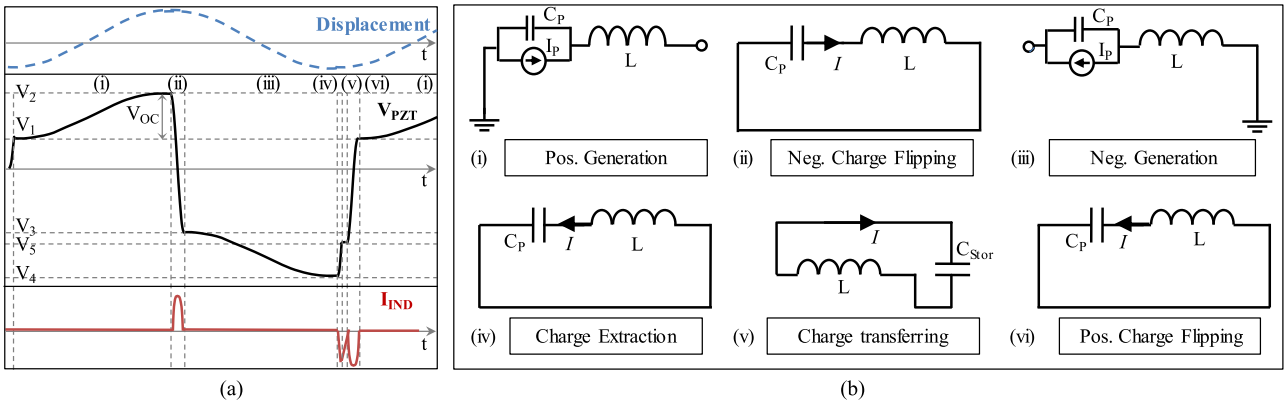

Fig. 3. (a) Voltage and current waveforms corresponding to (b) operation phases of the proposed switching circuits.

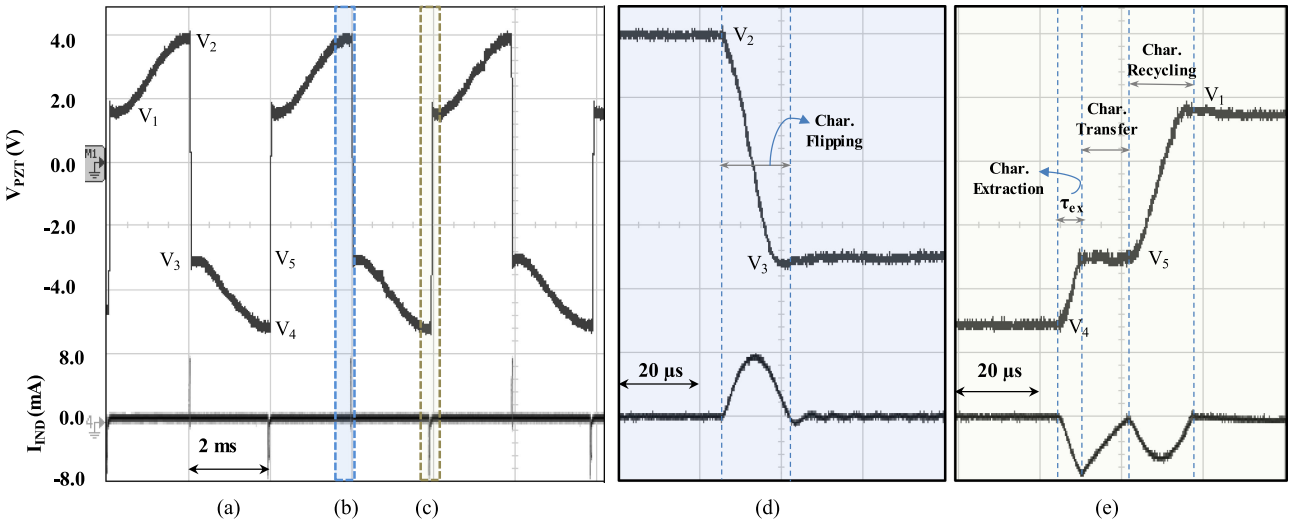

Fig. 4. Measured piezoelectric voltage and inductor current waveforms for (a) steady-state operation of SA-SSH interface circuit, (b) close up of charge-flipping instances, (c) close up of charge extraction and recycling instants (103YB PEH, $C_P = 15$ nF, $L = 3.3$ mH, $C_{\text{stor}} = 1$ μF).

after half an electrical period, resulting in the inversion of the peak voltage, $V_{\text{PN}} = -\lambda V_2$, called charge flipping.

3) Turning S_1 OFF while S_2 is ON starts negative charge generation phase by pushing charge to the V_N node from the inductor, and harvester negative current starts to charge C_P in the opposite direction.
4) Energy extraction is realized at minimum mechanical displacement by turning S_1 and S_2 ON.
5) A portion of the generated energy charges the inductor, after which point the circuit opens S_1 and closes S_3 to deliver the energy to the output capacitor. As inductor current crosses the zero point, S_3 is turned OFF to block current flow back.
6) The remaining generated energy is recycled into piezoelectric capacitor through positive charge flipping by turning both S_1 and S_2 ON. At the end of charge flipping, the circuit goes back to positive charge generation, and initiates the next cycle. The measured voltage and current waveforms during various phases are detailed in Fig. 4.

B. Optimal Energy Transfer

Extraction charge ratio, α, is defined to determine the values of the charge extracted, $\alpha C_p V_4$, and recycling charge in each period, $(1-\alpha)C_p V_4$, where V_4 indicates the voltage accumulated at minimum mechanical displacement. The maximum energy extraction can be achieved by tuning α. The proportion of voltage left on the capacitor C_p after discharging is a control parameter adjusted by the S_1 and S_2 switches. The optimum point depends on the Q factor of charge-flipping path, which in turn depends on piezoelectric capacitor, external inductor, as well as inductor and path resistance.

Let V_1 be the voltage on C_p just after charge flipping has occurred, and harvester starts generating charge on C_p in positive direction. $V_2 = V_1 + 2\frac{\Gamma}{C_P}U_m$ is the accumulated voltage

before charge flipping to negative voltage. Previously, λ is defined as the fraction of the voltage magnitude left after the charge flipping takes place, so the magnitude of the voltage after the flipping is $V_3 = -\lambda V_2$. V_4 is minimum voltage generated at a negative generation phase, and V_5 is the voltage left on C_p after the discharge takes place, such that $V_5 = \alpha V_4$. Then

$$V_3 = -\lambda(V_1 + 2\frac{\Gamma}{C_P}U_m) \tag{3}$$

$$V_4 = V_3 - V_{\rm oc} \tag{4}$$

$$V_5 = \alpha V_4 \tag{5}$$

$$V_1 = -\lambda V_5. \tag{6}$$

Substituting for V_5 from (5) into (6) and then for V_1 from (6) into (3) eliminates two variables. Finally, steady-state value of V_4 is derived from solving (3) to (4) as

$$V_4 = -2\frac{\Gamma}{C_P}\frac{1+\lambda}{1-\alpha\lambda^2}U_m. \tag{7}$$

During charge extraction phase 4, the current flow into the inductor is derived by governing equation of electric charge

$$L\ddot{q} + r\dot{q} + q/C_p = 0 \tag{8}$$

The initial charge is $C_P V_4$, yielding the current expression as

$$\dot{q} = C_P V_4 \frac{\omega_d}{\sqrt{1 - 1/4Q_f^2}} e^{-\frac{\omega_d}{Q_f}t} \sin(\omega_d t). \tag{9}$$

The charge extraction stops after a given time-interval, t_α, determined by α. The current expression at the end of this phase is given as $\dot{q}_{\rm ex,end} = \dot{q}\ (t_\alpha)$.

In the next phase, the energy stored at inductor is transferred to storage capacitor as a result of turning S_3 and S_2 ON. The differential equation for energy transfer phase, given the assumptions $C_{\rm stor} >> C_p$ and approximately constant storage voltage, yields

$$L\ddot{q}_t + r\dot{q}_t + V_{\rm stor} = 0 \tag{10}$$

where q_t is the transferred charge to the storage capacitor with initial condition of $\dot{q}_t(0) = \dot{q}_{\rm ex,end}$. At the end of charge transfer phase, $\dot{q}_t = 0$ as shown in Fig. 4. Assuming that voltage drop across $r_{\rm par}$ is negligible in comparison with $V_{\rm stor}$, allows the following approximation for the transferred charge:

$$\Delta q \approx \frac{1}{2}\frac{L}{V_{\rm stor}} q_{\rm ex,end}^2. \tag{11}$$

The extracted energy per cycle on the capacitor during discharge is

$$E = V_{\rm stor}\Delta q = \frac{1}{2}L q_{\rm ex,end}^2. \tag{12}$$

Using $\dot{q}_{\rm ex,end}$ expression and definition of α from above yields

$$E = \frac{1}{2}\eta_{\rm ex} C_p V_4 \left(1 - \alpha^2\right) \tag{13}$$

with $\eta_{\rm ex}$, the efficiency of energy extraction phase, given as

$$\eta_{\rm ex} = \frac{e^{-2\frac{\omega_d}{Q_f}t_\alpha}}{\sqrt{1 - 1/4Q_f^2}}. \tag{14}$$

Substituting for V_4 from (7) into (13) gives the extracted energy as a function of excitation level

$$E = 2\eta_{\rm ex}\left(1 - \alpha^2\right)\left(\frac{1+\lambda}{1-\alpha\lambda^2}\right)^2 \frac{\Gamma^2}{C_P} U_m^2. \tag{15}$$

Considering constant vibration magnitude, corresponding to low-coupled harvester or off-resonance excitation, differentiates *E* with respect to α to calculate the value of α that results in maximum *E*

$$\frac{dE}{d\alpha} = 0. \tag{16}$$

The value of extraction ratio that optimizes charge extraction is $\alpha_{\rm opt,CA} = \lambda^2$, giving the maximum extractable energy from the harvester as

$$E_{\max} = \frac{1}{2}\eta_{\rm ex}\frac{(1+\lambda)^2}{1-\lambda^4}\frac{\Gamma^2}{C_P}U_M^2. \tag{17}$$

Considering constant driving force magnitude, the energy balance of the system exposed to the external force F_M during the full period is expressed as

$$\int_0^T F\dot{u}dt = \int_0^T d\dot{u}^2 + \int_0^T \Gamma V \dot{u} dt. \tag{18}$$

The portion of the mechanical energy that is converted into transferred electrical energy can be expressed as the following integral function of voltage *V*, and displacement *u*

$$E_T = \int_{-U_m}^{U_M} \Gamma V du = 4U_m^2 \frac{\Gamma^2}{C_P}\frac{(1+\lambda)(1+\alpha\lambda)}{(1-\alpha\lambda^2)}. \tag{19}$$

Assuming that the displacement remains sinusoidal, displacement amplitude, U_M, is derived from the simplification of energy balance equation as a function of the external force amplitude F_M

$$U_m = \frac{F_M}{d\omega + \frac{4\Gamma^2}{\pi C_P}\frac{(1+\lambda)(1+\alpha\lambda)}{(1-\alpha\lambda^2)}}. \tag{20}$$

Substitution of (20) into (15) gives the extracted energy of the energy-harvesting system

$$E = 2\eta_{\rm ex}\frac{\kappa^2 Q_m}{\pi}\left(1-\alpha^2\right)\left(\frac{1+\lambda}{1-\alpha\lambda^2}\right)^2 \times \left(\frac{F_M}{1 + \frac{4}{\pi}\kappa^2 Q_m \frac{(1+\lambda)(1+\alpha\lambda)}{(1-\alpha\lambda^2)}}\right)^2. \tag{21}$$

The product of the squared coupling coefficient by the mechanical quality factor is defined as $\kappa^2 Q_m = \frac{\Gamma^2}{C_P d\omega_{\rm res}}$. The maximization of the extracted energy leads to optimal value of extraction ratio as

$$\alpha_{\rm opt,CF} = \frac{\lambda\left(\lambda - \frac{4}{\pi}\kappa^2 Q_m(1+\lambda)\right)}{1 + \frac{4}{\pi}\kappa^2 Q_m(1+\lambda)} \tag{22}$$

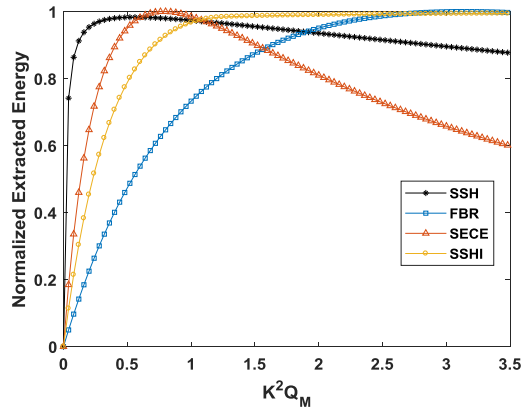

(a)

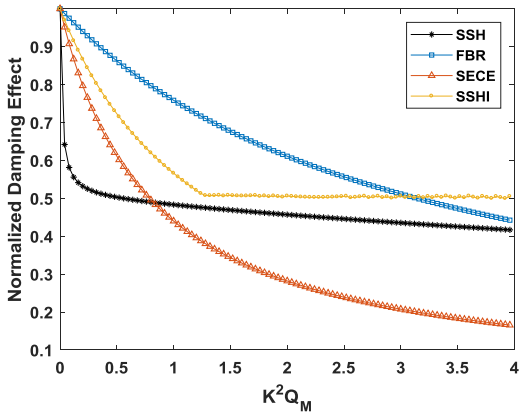

(b)

Fig. 5. (a) Normalized extracted energy and (b) damping effect versus $k^2Q_m(\lambda = 0.9)$.

and damping effect can be expressed as

$$\frac{(U_m)_{\text{SSH}}}{(U_{\text{mm}})_{\text{no extraction}}} = \frac{1}{1 + \frac{4}{\pi}\kappa^2 Q_m \frac{(1+\lambda)(1+\alpha\lambda)}{(1-\alpha\lambda^2)}} \tag{23}$$

with displacement where no energy is extracted from harvester.

Fig. 5(a) shows normalized extracted energy as a function of $\kappa^2 Q_m$ for optimum values of each technique. Fig. 5(b) depicts variations of damping effects as a function of $\kappa^2 Q_m$. The proposed approach provides higher extractable power for lower $\kappa^2 Q_m$ that is common for small-sized piezoelectric harvesters or off-resonance excitations. Indeed, this indicates that less-piezoelectric material is required with the proposed scheme to attain the same power-generation level. The maximum extractable power is achieved by adjusting charge extraction ratio, α, which controls the damping force of the piezoelectric harvester. As ascribed, the charge-flipping process has associated losses due to nonidealities in the inductor and switching, which affects extractable power. Fig. 6 depicts dependence of normalized extracted energy on charge-flipping ratio for both theoretical maximum and proposed scheme. Higher efficiency of the flipping provisions more power, obviously, perfect flipping $\lambda = 1$ can deliver maximum extractable power. For lower $\kappa^2 Q_m$ value, $\alpha_{\text{opt,CA}} = \lambda^2$ gives power close to the maximum extractable power ($\alpha_{\text{opt,CF}}$).

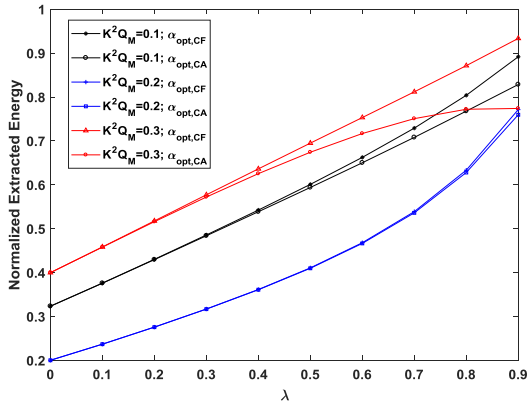

Fig. 6. Normalized extracted power dependency on λ and α variation.

III. Circuit Implementation

Fig. 7 shows the proposed circuit utilizing an external inductor, L, and a storage capacitor, C_{stor}. The power switches are implemented with thick-oxide 12 V MOSFETs to tolerate higher open-circuit (OC) voltages up to 6 V peak-to-peak that is swing on their terminals. There are three sources of power dissipation in the switching circuit. Resistive conduction losses in the inductors and MOSFET switches (P_{cond}); charge redistribution losses at MOSFET parasitic capacitances (P_{dist}); and capacitive switching losses at the gates of power switches (P_{sw}) during phase changes. The expressions of these losses are listed in Table I. Minimizing conduction loss at power switches plays a significant role in achieving higher Q. The widths of the power switches are set to $W_{S1,2} = 30$ mm and $W_{S3} = 14$ mm, which represent compromise across conduction losses due to ON resistance, switching losses due to gate-source capacitance, and charge redistribution at parasitic capacitances so as to minimize total power losses in the switching circuit. On the other hand, the building blocks are designed toward achieving optimal timing and minimization of power dissipation.

A. Peak Detectors

Fig. 8 shows configuration of the original high precision peak detector utilized to sense both positive and negative peaks with corresponding connections in the core circuit. The circuit operates in current mode to accommodate PEH voltages higher than its supply voltage. The input voltage is converted to current by a series capacitor, C_{PK}, in conjunction with internal negative feedback. With increasing piezoelectric voltage, the sensed current, I_S charges node V_X up to M_{N0} threshold voltage. The feedback through M_{P0} prevents further increase at V_X. As PEH voltage peaks, I_S reaches zero, and charge dissipation at node V_X by M_{P0} turns M_{N0} OFF. Voltage at node V_Y increases due to mirroring of the bias current. Common source amplifier and digital inverter at the output stage deliver a high edge rate. The bias current and the series capacitor values independently determine the upper limit of the input frequency and the minimum detectable amplitude, respectively. Details of this peak detector circuit have been reported in [13] with simulation and experimental results.

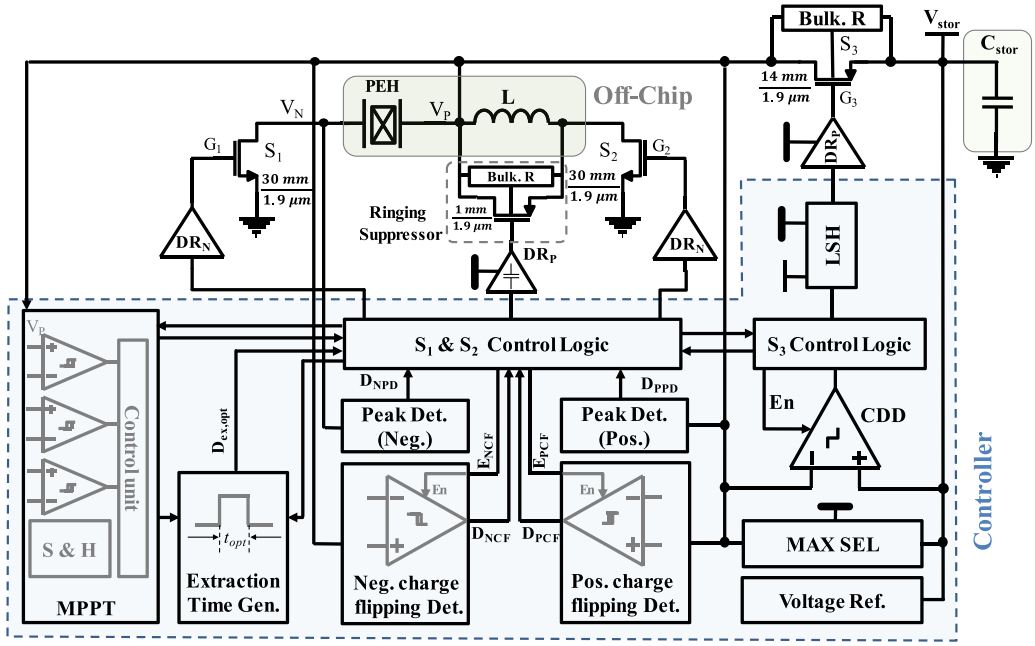

Fig. 7. Implementation of proposed optimal SA-SSH interface circuit.

TABLE I
COMPONENTS OF POWER LOSS

Loss source	Expression
Conduction	$P_{cond} = \left(\int_0^{t_f} r_f i_{f,(ii)}^2 dt + \int_0^{t_{ex}} r_f i_{ex,(iv)}^2 dt + \int_0^{t_{tran}} r_{tran} i_{tran,(v)}^2 dt + \int_0^{t_f} r_f i_{f,(vi)}^2 dt \right) \times f_{exc}$
Driving (Phase Change)	$P_{sw} = \underset{(i)(ii)}{C_{gs,S2} V_{Stor}^2 f_{exc}} + \underset{(iii)(iv)}{C_{gs,S1} V_{Stor}^2 f_{exc}} + \underset{(iv)(v)}{C_{gs,S3} V_{MAX}^2 f_{exc}} + \underset{(v)(vi)}{C_{gs,S1} V_{Stor}^2 f_{exc}}$
Charge Redistribution (Phase Change)	$P_{distr} = \underset{(i)(ii)}{C_{ds,S2} V_2^2 f_{exc}} + \underset{(iii)(iv)}{C_{ds,S1} V_4^2 f_{exc}} + \underset{(v)(vi)}{C_{ds,S2} (V_{Stor} - V_5)^2 f_{exc}}$

$r_f = r_{ind} + r_{s1} + r_{s2}$, $r_{ex} = r_{ind} + r_{s2} + r_{s3}$, where r_{s1}, r_{s2}, and r_{s3} are ON resistors of the switches, i_f is the current of the filliping circuit as Eq. (9) corresponding to each phase, $C_{gs,S1}$, $C_{gs,S2}$, *and* $C_{gs,S3}$ are the gate capacitance of the switches, $C_{ds,S1}$ *and* $C_{ds,S2}$ are the equivalent parasitic capacitance at drain of S_1 and S_2.

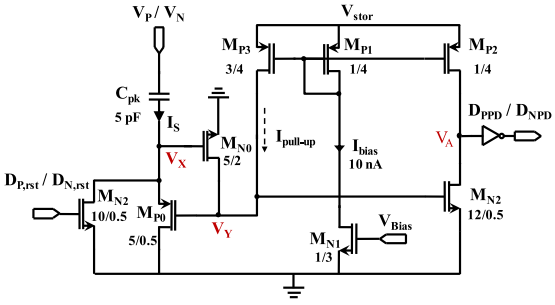

Fig. 8. Schematic of the implemented peak detector.

B. Charge-Flipping Sensor

The charge-flipping action is accomplished when all charge transferred to the inductor flows back into the piezoelectric capacitance, C_P. The circuit presented in Fig. 9(a) detects the depletion point by sensing the current that piezoelectric voltage induces on the C_{sens} capacitor. The voltage–current conversion is realized using a flipped voltage follower (FVF) circuit that provides low input impedance and low input voltage requirements with the feedback connection of M_1 and M_3 at the drain of M_1. This circuit retains a roughly constant voltage at V_C node. The sensed current, I_{sens}, plus bias current, I_{bias}, replicated at P-type metal-oxide-semiconductor (PMOS) M_1–M_3 through a current mirror, establish the sensed voltage V_S across resistor R_s in proportion to the sensed current. V_S is compared with offset voltage, V_{ref}, generated with mirrored bias current across the reference resistor, $R_{\text{ref}} = R_s$. While the current on the external inductor flows into the piezoelectric capacitance C_P, higher voltage at the inverting input of the comparator keeps previous state of the comparator. Just as no energy remains to drain from the external inductor, the current flowing into C_S becomes zero, and eventually the voltage established at R_S falls below V_{ref} that

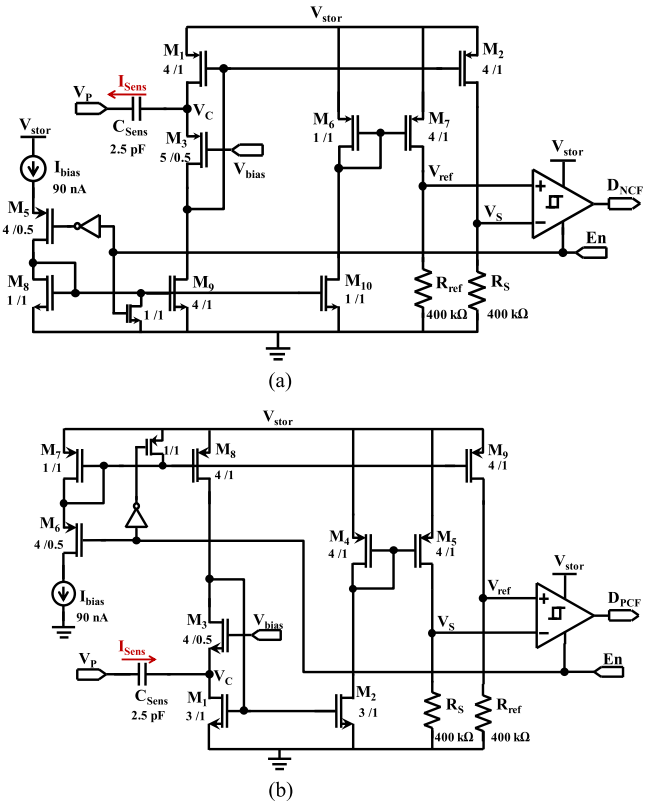

Fig. 9. Schematic of (a) negative charge-flipping sensor, and (b) positive charge-flipping sensor.

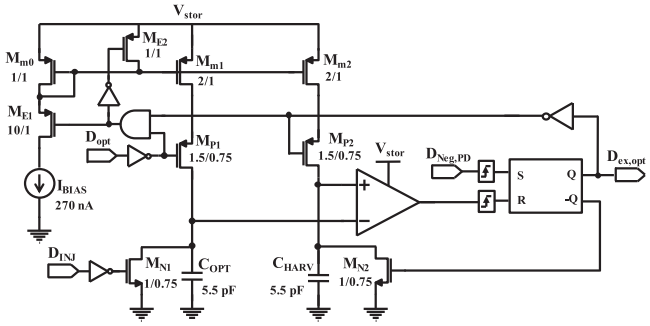

Fig. 10. Schematic of implemented extraction time generator.

changes the state of the comparator from low to high. The positive charge flip is similarly detected with the circuit shown in Fig. 9(b). The proposed method with FVF circuit helps to sense nano ampere range of current variation precisely and wideband comparator provides fast and high accuracy detection as seen in Fig. 4(b) and (c).

C. Extraction Time Generator

Extraction time generator, implemented as shown in Fig. 10, saves optimum extraction time in MPPT mode and regenerates its each cycle in operation mode. During MPPT mode, D_{OPT} turns M_{P1} switch ON to allow reference current flows through

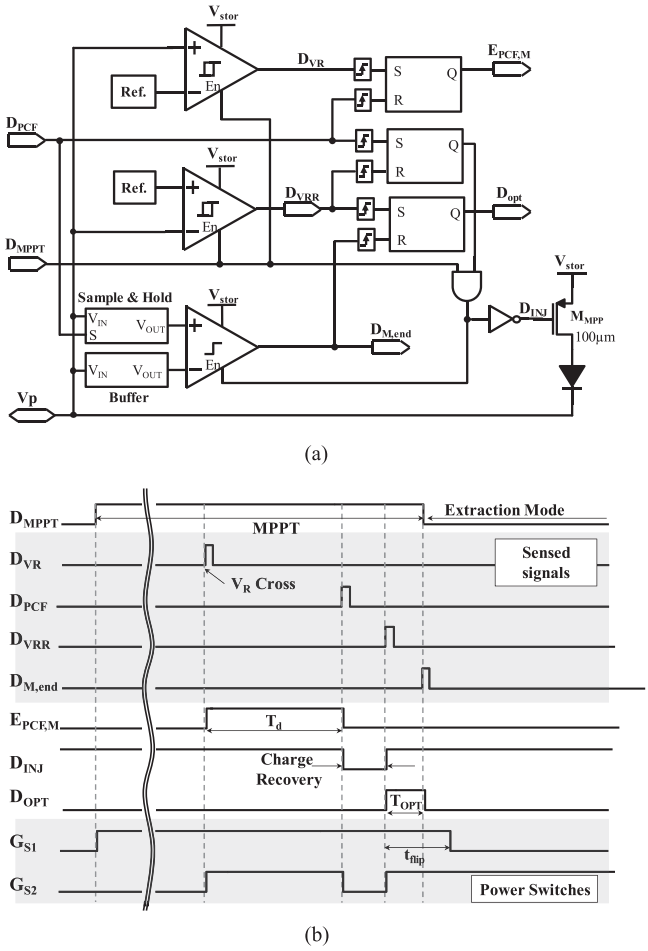

Fig. 11. (a) MPPT circuit and (b) corresponding signal waveforms.

M_{P1} into C_{opt} to set the optimum extraction time as a reference voltage, V_{OPT}. In extraction mode, when negative peak detector's output goes high, control unit initiates rising edge of $D_{\mathrm{ex,opt}}$ pulse and closes switch M_{P2} to steer reference current into C_{HARV}. The generated ramp voltage, V_{HARV}, is compared with V_{OPT}, corresponding to the optimum extraction time, to reset SR latch and generate falling edge of the extraction time signal. Then, C_{harv} is discharged through M_{N2} MOSFET to reset for the next cycle.

D. Charge Depletion Detection (CDD)

Depletion of extracted energy from the inductor to the storage capacitance is controlled by a charge-depletion comparator with a relatively high bandwidth. A conventional two-stage comparator monitors the voltage across S_3 switch (Fig. 7) to detect the end of inductor energy discharging. The control unit activates the CDD only in charge transferring phase as a design compromise between power consumption and comparator bandwidth. The output signal of the CCD ends the charge transferring and initiates charge-recycling phase.

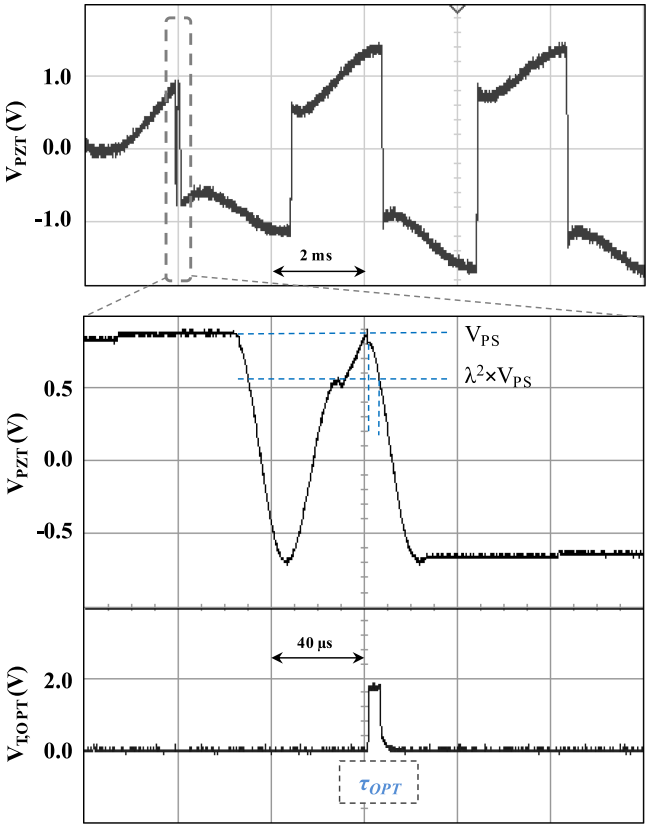

Fig. 12. Measured waveforms of optimum power point detection (103YB PEH, $C_P = 15$ nF, $L = 3.3$ mH, $C_{\text{stor}} = 1$ μF).

TABLE II
BREAK DOWN OF CONTROL LOSSES ($V_{\text{stor}} = 2.75$ V, $L = 3.3$ MH, $f_{\text{exc}} = 254$ HZ)

Loss Mechanism	Power loss (nW)	Percentage
Voltage Reference	112	10.30%
Peak Detector	105	9.66%
Charge Flipping Detectors	74	6.80%
Reverse Current Detector	27	2.50%
Extraction Time Generator	124	11.40%
Switch Control	645.1	59.34%
Simulated Total	1087	100%
Measured Static Power	262	-
Measured Total	1310	-

E. MPPT Circuit

The optimum extraction time is achieved as $t_{\text{ex,opt}} = \frac{1}{\omega_d}\cos^{-1}(\lambda^2)$, corresponding to optimum charge extraction ratio $\alpha = \lambda^2$ and extraction phase, $V_5 = \lambda^2 V_4 = V_4 \cos(\omega_d t_{\text{ex,opt}})$. This leads to the elimination of input voltage variation, and identification of the MPP through optimum extraction time ($t_{\text{ex,opt}}$) measurement. Fig. 11 illustrates the schematic of the novel

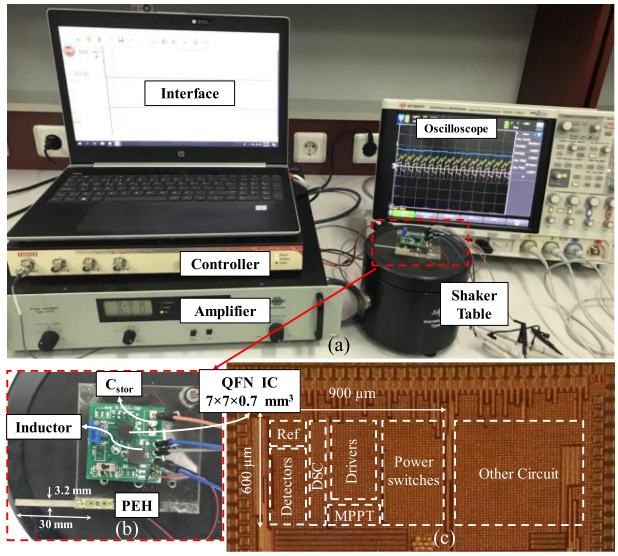

Fig. 13. (a) Experimental setup. (b) Evaluation board. (c) Die microphotograph.

MPPT circuit with corresponding signal waveforms. The proposed MPPT circuit enables the piezoelectric voltage to reach a reference voltage level, V_R. V_R is selected below minimum required storage voltage for proper operation. At this point, S_1 and S_2 turn ON to establish the resonant circuit. After one cycle of resonance period, T_d, λ^2 of initial voltage, V_R, is conserved on C_P because of damping. This point is detected by positive charge-flipping sensor, and piezoelectric voltage, $\lambda^2 \times V_R$, is sampled and held for comparison in the next step. Then, S_2 turns OFF. Charge is injected into C_p from storage devices through a control switch and a diode to recover piezoelectric voltage to V_R. At this moment, S_2 closes to establish the resonant circuit once more with the same initial voltage on C_P. The transient piezoelectric voltage is compared with sampled voltage to determine optimum extraction time corresponding to λ^2. The measured pulse, T_{opt}, is saved by time generator circuit to reproduce it in operation mode. Any process variations in flipping loop circuit is measured within optimum extraction time. Besides, the propagation delay of the driver is also considered and compensated for measuring given time points.

After finding the MPP in a cycle, the system initiates harvesting operation mode and switching is executed as defined previously. All phases of sensing the MPP are completed over one cycle of the mechanical vibration. Besides, excitation frequency and level do not affect the MPP. As result, the interface circuit provides maximum power extraction, independent of input vibration. Fig. 12 shows measured piezoelectric voltage and optimum extraction time in MPPT mode as illustrated in Fig. 11.

IV. DESIGN VALIDATION

The self-adapting SSH circuit is fabricated in 180 nm HV CMOS technology with 900 μm $\times$ 600 μm active area. Experimental setup, evaluation board, and microphotograph of the

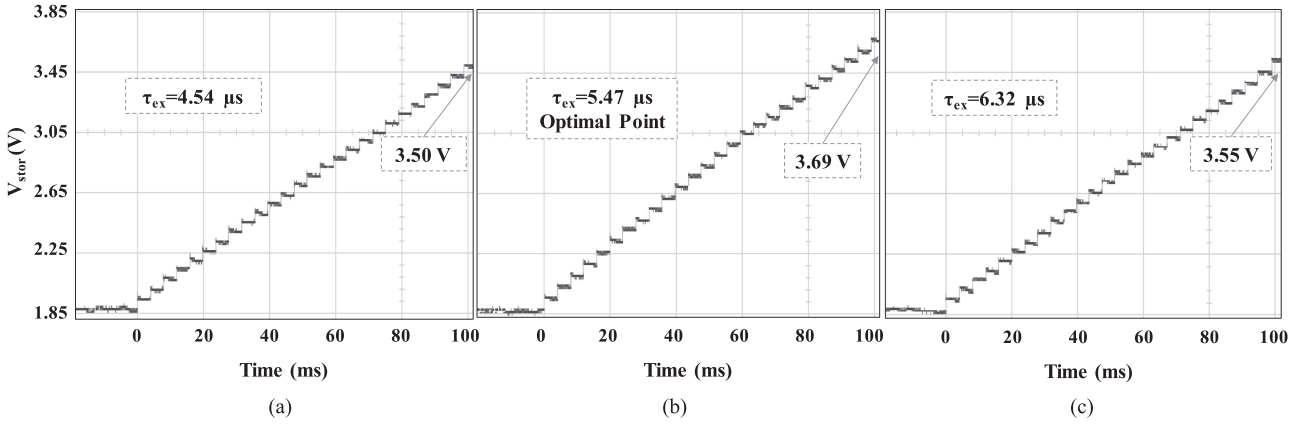

Fig. 14. Measured charge of storage capacitance with $V_{\mathrm{OC,pp}} = 2\,\mathrm{V}$ across charge extraction time (a) $\tau_{\mathrm{ex}} = 4.54\ \mu\mathrm{s}$ (b) $\tau_{\mathrm{ex,opt}} = 5.47\ \mu\mathrm{s}$ (c) $\tau_{\mathrm{ex}} = 6.32\ \mu\mathrm{s}$ (103YB PEH, $C_P = 15\,\mathrm{nF}$, $L = 3.3\,\mathrm{mH}$, $C_{\mathrm{stor}} = 1\ \mu\mathrm{F}$, $R_L = 10\,\mathrm{M\Omega}$).

chip are depicted in Fig. 13. An off the shelf 103YB cantilever PEH from Piezo System has been mounted on a shaker table and a 1 μF storage capacitor at output for measurements, as shown in Fig. 13. The cantilever PEH with 28.6 mm $\times$ 3.2 mm dimensions has an output capacitance of 15 nF, and resonance frequency of 253 Hz.

The average power consumption per building block in the implemented IC is listed in Table II. These figures are simulation results while PEH is excited at 253 Hz with $V_{\mathrm{OC}} = 2.2\,\mathrm{V}$. The static power loss is measured by fixing $V_{\mathrm{stor}} = 2.75$ through an external supply and measuring the drawn current while the IC is not performing any energy extraction. The total power loss is measured as PEH vibrates at 253 Hz. The average dynamic power loss of the building blocks is affected by the external inductor value and exciting frequency. The total control loss is about 5% of the output power (19.75 μW) at $V_{\mathrm{OC}} = 2.24\,\mathrm{V}$, and forms an even smaller fraction of the generated power for higher excitation levels.

The optimal charge performance of the energy harvesting system is evaluated by manually tuning extraction time, τ_{ex}, as depicted in Fig. 14 with $C_{\mathrm{stor}} = 1\ \mu\mathrm{F}$, for 253 Hz PEH stimulation and 2 V peak-to-peak amplitude. The initial value of the output buffer is set to 1.85 V for safe operation. The employed MPP yields the fastest charge performance in comparison with shorter and longer extraction times. Shortened extraction time, $\tau_{\mathrm{ex}} = 4.54\ \mu\mathrm{s}$, harvests smaller amount of the generated charge and reinjects more charge into C_p, which limits energy conversion due to power losses. On the other hand, raising τ_{ex} to 6.31 μs decreases recycling charge into piezoelectric capacitance, and consequently reduces the contribution of the damping force.

The power delivered to 1 μF storage capacitor in parallel with a variable load resistor has been measured for different excitation levels. The extracted and output powers as a function of the storage voltage are shown in Fig. 15 for $V_{\mathrm{OC,pp}} = 2.24\,\mathrm{V}$, $V_{\mathrm{OC,pp}} = 3.4\,\mathrm{V}$, and $V_{\mathrm{OC,pp}} = 5.6\,\mathrm{V}$. The dependence of the extracted output power on storage voltage is low, as expected, because of the switching technique that decouples the PEH and storage device during energy extraction. Fig. 16 shows

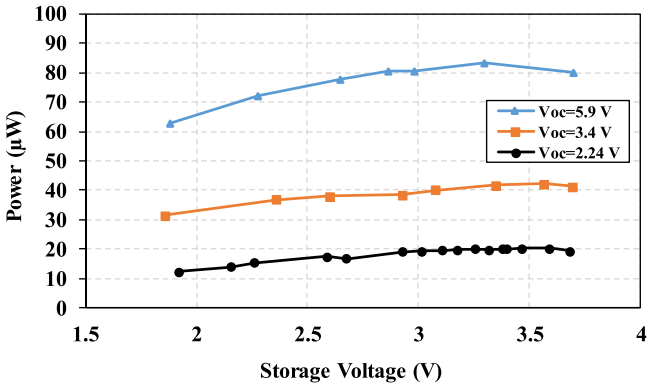

Fig. 15. Measured output power versus output dc storage voltage for $V_{\mathrm{OC,pp}} = 2.24\,\mathrm{V}$ and $V_{\mathrm{OC,pp}} = 5.9\,\mathrm{V}$ (103YB PEH, $C_p = 15\,\mathrm{nF}$, $L = 3.3\,\mathrm{mH}$, $C_{\mathrm{stor}} = 1\ \mu\mathrm{F}$).

the delivered power to storage element, P_{stor}, as a function of OC piezoelectric voltages for three different external inductor values. The proposed IC harvests 21.3 μW from cantilever PEH at $V_{\mathrm{OC,pp}} = 2.24\,\mathrm{V}$ with 3.3 mH, and enhances stored power 4.53 times compared to a lossless full-wave bridge rectifier, which delivers 4.7 μW onto optimum load resistance from the same vibration. Smaller inductors have reduced power gain as OC voltage of the PEH increases, due to the increase in power losses with excitation level.

The power measurements are also conducted for custom-made MEMS PEH mounted on a shaker table with output capacitance of 2 nF, resonance frequency of 317 Hz, and 9 mm $\times$ 4 mm footprint. The harvested power, P_{stor}, and associated Figure of merit (FOM) as a function of OC piezoelectric voltage, $V_{\mathrm{OC,pp}}$, is depicted in Fig. 17 with 1 mH/ 5.1 Ω external inductor for both proposed circuit and conventional SECE IC. FOM compares P_{stor} against the maximum power extractable by a lossless full-bridge rectifier as

$$\mathrm{FOM} = \frac{P_{\mathrm{stor}}}{f_{\mathrm{exc}} C_p V_{\mathrm{oc}}^2}. \tag{24}$$

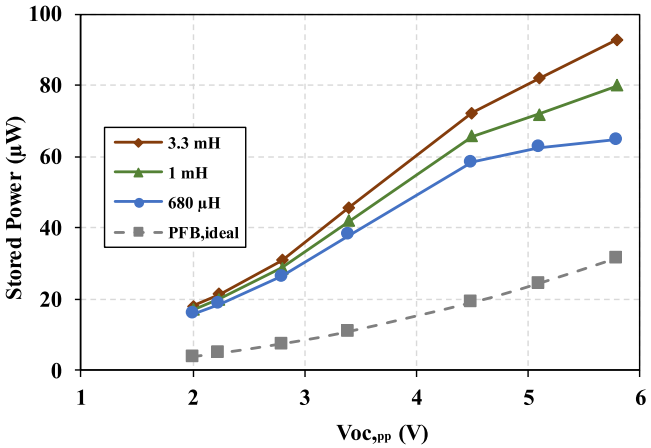

Fig. 16. Measured extracted power versus excitation OC piezoelectric voltage for three different external inductors (103YB PEH, $C_P = 15$ nF, $L = 3.3$ mH, $C_{\text{stor}} = 1$ μF).

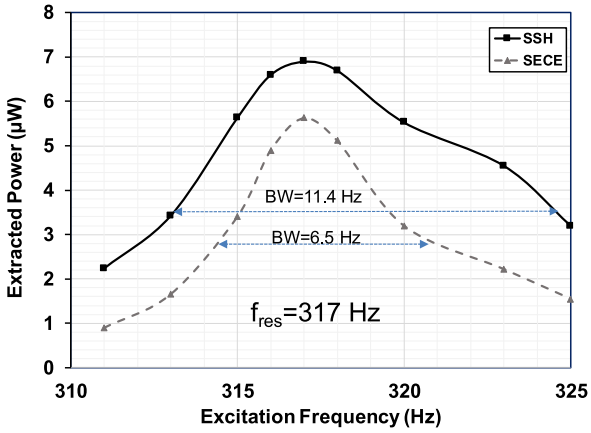

Fig. 18. Measured harvested power versus frequency with 1 g excitation.

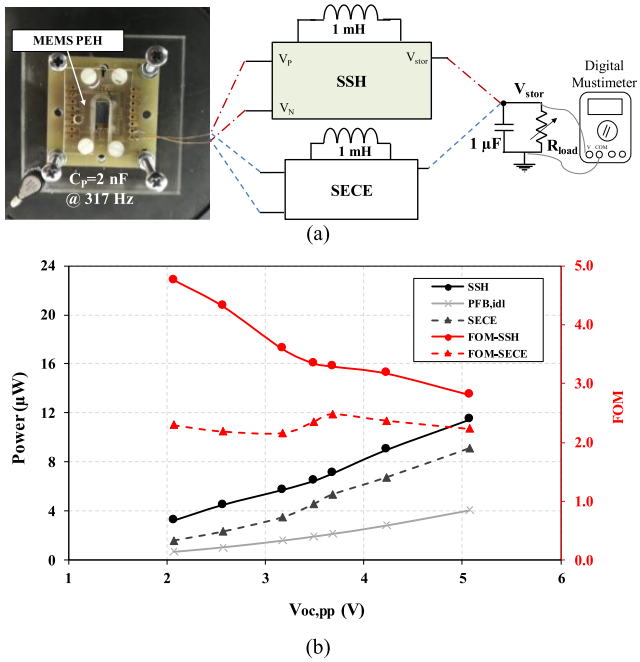

Fig. 17. Measured harvested power from custom-made MEMS PEH by the proposed IC compared to SECE IC and ideal full-bridge rectifier at different excitation levels ($C_P = 2$ nF, $C_{\text{stor}} = 1$ μF).

The FOM has been defined previously in [24], [27], [28]. An FOM of 4.75 is achieved with 1 mH inductor. This power gain is due to the lower coupling-factor of the MEMS PEH, where the performance of the full-wave rectifier is severely affected, while the proposed IC with MPPT circuit excels. The proposed IC shows better power performance in comparison with SECE counterparts. As expected, the IC extracts more power especially at low excitation levels as the circuit controls the damping force more efficiently. Fig. 18 shows the harvested power both for the proposed circuit and the conventional SECE, as a function of excitation frequency at 1 g acceleration with 1 mH/ 5.1 Ω external inductor. The presented circuit harvests 22% more power at resonance frequency, and up to100% more power at off-resonance frequencies in comparison with SECE circuit. Besides, the 3 dB bandwidth of the harvesting system is extended 75% over that of the SECE, which is a significant advantage as the excitation frequency or resonance frequency drifts in the environment of real applications. Thus, the proposed technique facilitates miniaturization of piezoelectric harvesting structure for a targeted energy-generation rate.

Table III compares characteristics and performance of the proposed IC against recent piezoelectric energy-harvesting ICs. Kwon [28] used external tunable delay to invest from battery into piezoelectric harvester that should be adjusted exclusively for each vibration strength. The investment technique loses its efficiency at weak and damped vibrations. Contrary to [28], the proposed IC shows higher FOM, in weak vibrations, and is highly efficient in response to damped vibration. The conventional SSHI techniques [24], [29] utilized bulky inductors to achieve higher charge inversion efficiency, while our system utilizes 1 mH inductor within a small-sized package (67 mm^3) to reduce volume and cost with FOM of 4.75. SSHC interfaces [26], [27] benefit from capacitor-based flipping design that leads to smaller system volume; however, this scheme requires capacitors that are proportionate in value to the piezoelectric capacitor, has additional losses, and external calibration of charge-flipping circuit is needed to obtain high flipping ratio. The presented chip automatically adjusts charge-flipping time and optimal extraction point, which make the system robust in terms of adaptation. The ultra-low power consumption enables power extraction from low-level vibrations, where SSHC techniques suffer from low conversion efficiency. In contrast to SSHI and SSHC, the presented IC does not require a buffer voltage converter to achieve maximum efficiency. On the other hand, the IC presents improved bandwidth and chip area over SECE and other techniques. This IC, with associated MPPT technique, paves the way toward automatic and efficient power converters for low-coupled transducers such as MEMS PEHs, while using only a low-profile off-chip inductor. This IC, along with MPPT technique, paves the way towards automatic and efficient power

TABLE III
COMPARISON OF PROPOSED IC WITH STATE OF THE ART

Ref.	Process CMOS	Chip area (mm^2)	C_p (nF)	V_{OC} (V)	f_{exc} (Hz)	Inductor/ Capacitor	Inductor Size (mm^3)	P_{stor} (μW)	FOM	MPP [Fliping]
[24] SSHI	0.18 µm	0.1	3.52	3	220	1000 µH	-	4.61	2.65*	- [Ext. adj.]
[28] Investment	0.35 µm	1.80×1.30	15	2.6	143	330 µH	416	52	3.59	- [Ext. adj.]
[15] SECE	180 nm	0.55	43	5.69	75.4	2200 µH	-	82.6	3.14	- [Self-adj.]
[29] SSHI	0.35 µm	1.20	9	0.95	229	3300 µH	29650	8.19	4.40	Ext. adj. [Ext. adj.]
[25] SSHI	0.32 µm	0.98×0.76	19	4.9	144	220 µH	-	136	2.07	- [Self-adj.]
[26] FCR	180 nm	1.7	0.08		110,000	-	-	50.2	4.78**	- [Ext. adj.]
[27] SSHC	0.35 µm	2.9	45	2.5	92	8 × 45 nF	-	161.8	6.3*	- [Ext. adj.]
This work Opt. SSH	**180 nm**	**0.90×0.60**	**2**	**1.12**	**317**	**1000 µH**	**67**	**3.22**	**4.75**	**MPP [Self-adj.]**

converters for low-coupled transducers such as MEMS PEHs while using only a small-sized off-chip inductor.

V. CONCLUSION

A piezoelectric energy-harvesting IC has been designed and implemented in 180 nm CMOS technology for harnessing energy from ambient vibration sources. A novel synchronized switching configuration with an MPPT circuit has been proposed to boost extracted energy from PEHs, and provide load-independent energy extraction with a single inductor. The IC achieves maximum power gain of 5 at output power of 3.4 μW compared with ideal full-bridge rectifier that harnesses 0.678 μW for the same vibration strength. The experimental result shows that IC can harvest energy efficiently from different harvesters and inductors without external tuning, as system adjusts optimum operation point automatically regardless of the variation in the available energy on PEH. The presented IC delivers the utmost extractable energy to storage element, which is a significant contribution for the realization of the energy-harvesting microdevices for wireless sensors or biomedical applications.

REFERENCES

[1] P. D. Mitcheson, E. M. Yeatman, G. K. Rao, A. S. Holmes, and T. C. Green, "Energy harvesting from human and machine motion for wireless electronic devices," in *Proc. IEEE*, 2008, vol. 96, no. 9, pp. 1457–1486.

[2] G. T. Hwang, M. Byun, C. K. Jeong, and K. J. Lee, "Flexible piezoelectric thin-film energy harvesters and nanosensors for biomedical applications," *Adv. Healthc. Mater.*, vol. 4, no. 5, pp. 646–658, 2015.

[3] L. Beker, O. Zorlu, N. Goksu, and H. Kulah, "Stimulating auditory nerve with MEMS harvesters for fully implantable and self-powered cochlear implants," in *Proc. Transducers Eurosensors XXVII: 17th Int. Conf. Solid-State Sensors, Actuators Microsystems,* 2013, pp. 1663–1666.

[4] E. E. Aktakka, *Integration of Bulk Piezoelectric Materials Into Microsystems*. Ann Arbor, MI, USA: Univ. Michigan, 2012.

[5] T. T. Le, J. Han, A. Von Jouanne, K. Mayaram, and T. S. Fiez, "Piezoelectric micro-power generation interface circuits," *IEEE J. Solid-State Circuits*, vol. 41, pp. 1411–1419, 2006.

[6] Y. Kushino and K. Koizumi, "Piezoelectric energy harvesting circuit using full-wave voltage doubler rectifier and switched inductor," in *Proc. IEEE Energy Convers. Congr. Expo.*, 2014, pp. 2310–2315.

[7] Y. Lam, W. Ki, and C. Tsui, "Integrated low-loss CMOS active rectifier for wirelessly powered devices," *Simulation*, vol. 53, no. 12, pp. 1378–1382, 2006.

[8] W. Jingmin, Y. Zheng, Z. Zhangming, and Y. Yintang, "An ultra-low-voltage rectifier for PE energy harvesting applications," *J. Semicond.*, vol. 37, no. 2, pp. 25004-1-25004–5, 2016.

[9] M. Shim, S. Member, J. Kim, and S. Member, "Self-powered 30 μW to 10 mW piezoelectric energy harvesting system with 9.09 ms/V maximum power point tracking time," *IEEE J. Solid-State Circuits*, vol. 50, no. 10, pp. 2367–2379, Oct. 2015.

[10] N. Kong and D. S. Ha, "Low-power design of a self-powered piezoelectric energy harvesting system with maximum power point tracking," *IEEE Trans. Power Electron.*, vol. 27, no. 5, pp. 2298–2308, May 2012.

[11] E. Lefeuvre, A. Badel, C. Richard, L. Petit, and D. Guyomar, "A comparison between several vibration-powered piezoelectric generators for standalone systems," *Sensors Actuators, A Phys.*, vol. 126, pp. 405–416, 2006.

[12] J. Dicken, P. D. Mitcheson, S. Member, I. Stoianov, and E. M. Yeatman, "Power-extraction circuits for piezoelectric energy harvesters in miniature and low-power applications," *IEEE Trans. Power Electron. Electron.*, vol. 27, no. 11, pp. 4514–4529, Nov. 2012.

[13] S. Chamanian, H. Ulusan, A. Koyuncuoglu, A. Muhtaroglu, and H. Kulah, "An adaptable interface circuit with multi-stage energy extraction for low power piezoelectric energy harvesting MEMS," *IEEE Trans. Power Electron.*, vol. 34, no. 3, pp. 2739–2747, Mar. 2018.

[14] T. Hehn *et al.*, "A fully autonomous integrated interface circuit for piezoelectric harvesters," *IEEE J. Solid-State Circuits*, vol. 47, no. 9, pp. 2185–2198, Sep. 2012.

[15] A. Morel *et al.*, "A shock-optimized SECE integrated circuit," *IEEE J. Solid-State Circuits*, vol. 53, no. 12, pp. 3420–3433, Dec. 2018.

[16] A. Badel, D. Guyomar, E. Lefeuvre, and C. Richard, "Efficiency enhancement of a piezoelectric energy harvesting device in pulsed operation by synchronous charge inversion," *J. Intell. Mater. Syst. Struct.*, vol. 16, no. 10, pp. 889–901, 2005.

[17] L. Garbuio, M. Lallart, D. Guyomar, C. Richard, and D. Audigier, "Mechanical energy harvester with ultralow threshold rectification based on SSHI nonlinear technique," *IEEE Trans. Ind. Electron.*, vol. 56, no. 4, pp. 1048–1056, Apr. 2009.

[18] M. Lallart, C. Richard, L. Garbuio, L. Petit, and D. Guyomar, "High efficiency, wide load bandwidth piezoelectric energy scavenging by a hybrid nonlinear approach," *Sensors Actuators, A Phys.*, vol. 165, no. 2, pp. 294–302, 2011.

[19] Y. K. Ramadass and A. P. Chandrakasan, "An efficient piezoelectric energy harvesting interface circuit using a bias-flip rectifier and shared inductor," *IEEE J. Solid-State Circuits*, vol. 45, no. 1, pp. 189–204, Jan. 2010.

[20] E. E. Aktakka and K. Najafi, "A micro inertial energy harvesting platform with self-supplied power management circuit for autonomous wireless sensor nodes," *IEEE J. Solid-State Circuits*, vol. 49, no. 9, pp. 2017–2029, Sep. 2014.
[21] X. D. Do, H. H. Nguyen, S. K. Han, and S. G. Lee, "A rectifier for piezoelectric energy harvesting system with series synchronized switch harvesting inductor," in *Proc. IEEE Asian Solid-State Circuits Conf.*, 2013, pp. 269–272.
[22] D. A. Sanchez, J. Leicht, F. Hagedorn, E. Jodka, E. Fazel, and Y. Manoli, "A parallel-SSHI rectifier for piezoelectric energy harvesting of periodic and shock excitations," *IEEE J. Solid-State Circuits*, vol. 51, no. 12, pp. 2867–2879, Dec. 2016.
[23] S. Du, G. A. J. Amaratunga, and A. A. Seshia, "A cold-startup SSHI rectifier for piezoelectric energy harvesters with increased open-circuit voltage," *IEEE Trans. Power Electron.*, vol. 34, no. 1, pp. 263–274, Jan. 2018.
[24] S. Du, Y. Jia, C. Zhao, G. A. J. Amaratunga, and A. A. Seshia, "A passive design scheme to increase the rectified power of piezoelectric energy harvesters," *IEEE Trans. Ind. Electron.*, vol. 65, no. 9, pp. 7095–7105, Sep. 2018.
[25] L. Wu, X. D. Do, S. G. Lee, and D. S. Ha, "A self-powered and optimal SSHI circuit integrated with an active rectifier for piezoelectric energy harvesting," *IEEE Trans. Circuits Syst. I Regul. Pap.*, vol. 64, no. 3, pp. 537–549, Mar. 2017.
[26] Z. Chen, M. K. Law, P. I. Mak, W. H. Ki, and R. P. Martins, "A 1.7 mm^2 inductorless fully integrated flipping-capacitor rectifier (FCR) for piezoelectric energy harvesting with 483% power-extraction enhancement," in *Proc. IEEE Int. Solid-State Circuits Conf.*, 2017, vol. 60, pp. 372–373.
[27] S. Du and A. A. Seshia, "An inductorless bias-flip rectifier for piezoelectric energy harvesting,' *IEEE J. Solid-State Circuits*, vol. 52, no. 10, pp. 2746–2757, Oct. 2017.
[28] D. Kwon and G. A. Rincon-Mora, "A single-inductor 0.35 μm CMOS energy-investing piezoelectric harvester," *IEEE J. Solid-State Circuits*, vol. 49, no. 10, pp. 2277–2291, Oct. 2014.
[29] D. A. Sanchez, J. Leicht, E. Jodka, E. Fazel, and Y. Manoli, "A 4 μW-to-1mW parallel-SSHI rectifier for piezoelectric energy harvesting of periodic and shock excitations with inductor sharing, cold start-up and up to 681% power extraction improvement," in *Proc. IEEE Int. Solid-State Circuits Conf.*, 2016, vol. 59, pp. 366–367.

Salar Chamanian (M'17) received the B.Sc. (Hons.) and M.Sc. (Hons.) degrees in electrical and electronics engineering from the University of Tabriz, Tabriz, Iran, in 2009 and 2012, respectively. He received the Ph.D. degree in electrical engineering from the Middle East Technical University (METU), Ankara, Turkey, in 2018.

He is currently a Research Fellow with the Department of Electrical Engineering, METU. His research interests include complimentary metal–oxide–semiconductor integrated circuit design for low-power applications, interface electronics for energy harvester systems, sensors and actuators, power management circuit for wireless sensor network, and MEMS-based energy harvesters.

Ali Muhtaroglu (SM'06) received the B.S. degree from the University of Rochester, Rochester, NY, USA, in 1994, the M.S. degree from Cornell University, Ithaca, NY, USA, in 1996, and the Ph.D. degree from Oregon State University, Corvallis, OR, USA, in 2007, all in electrical engineering.

He was with Intel Corporation R&D, USA for 11 years before joining Electrical-Electronics Engineering at Middle East Technical University via Northern Cyprus Campus, Mersin, Turkey, in 2007, as a faculty member. His experience and research interests include integrated circuit design, energy harvesting, and low-power system architecture.

Dr. Muhtaroglu has numerous publications and a number of patents. He has chaired, cochaired, and served on the technical program committees for various IEEE conferences. He is currently chairing the Center for Sustainability at METU NCC.

Haluk Külah (M'97) received the B.Sc. (Hons.) and M.Sc. (Hons.) degrees in electrical engineering from Middle East Technical University (METU), Ankara, Turkey, in 1996 and 1998, respectively. He received the Ph.D. degree in electrical engineering from the University of Michigan, Ann Arbor, MI, USA, in 2003.

During his Ph.D., he worked on micromachined inertial sensors and their interface electronics. His interface electronics designs received several awards in design contests organized/sponsored by prestigious institutions including by DAC (Design Automation Conference), IBM, Analog Devices, Compaq, and Texas Instruments. From 2003 to 2004, he was a Research Fellow with the Department of Electrical Engineering and Computer Science, University of Michigan. He joined the Electrical and Electronics Engineering Department, METU, as a Faculty Member in August 2004. He has been the Deputy Director of METU-MEMS Research and Applications Center since 2008. He has authored/coauthored more than 130 international publications, 23 national/international patents, and eight international patent applications. His research interests include MEMS, MEMS-based energy scavenging, microsystems for biomedical applications (BioMEMS), and mixed-signal interface electronics design for MEMS sensors.

Dr. Külah has been awarded with 2009 Research Encouragement Award by Prof. Mustafa PARLAR Education and Research Foundation, 2013 Research Encouragement Award by TÜBİTAK, 2013 IBM Faculty Award, and 2015 Young Scientist Award by Turkish Science Academy. He has received 2015 ERC Consolidator Grant by FLAMENCO project, which is on autonomous and fully implantable cochlear implants.